

## Corrosion Inhibition of Carbon Steel in HCl and H<sub>2</sub>SO<sub>4</sub> Acids by Novel 1,3,4-Thiadiazolium-2-Phenylamine Salts

*Cristiane Frauches-Santos, Glauco F. Bauerfeldt, Aurea Echevarria\**

Departamento de Química, Instituto de Ciências Exatas, Universidade Federal Rural do Rio de Janeiro, Seropédica, RJ, 23851-900, Brazil

\*E-mail: [echevarr@hotmail.com](mailto:echevarr@hotmail.com)

*Received: 27 March 2018 / Accepted: 7 May 2018 / Published: 5 June 2018*

---

The inhibition ability of four 1,3,4-thiadiazolium-2-phenylamine chlorides (MI 1-4) towards carbon steel corrosion in 1.0 M HCl and 0.5 M H<sub>2</sub>SO<sub>4</sub> was evaluated by potentiodynamic polarization (PP), the linear resistance to polarization (LRP) and electrochemical impedance spectroscopy (EIS) at different inhibitor concentrations. Polarization curves showed that all the evaluated compounds act as mixed inhibitors with a tendency to become anodic in both acids. EIS plots indicated that the presence of all compounds increases the charge transfer resistance of the corrosion process, thus increasing the corrosion inhibition efficiency in both acids. These derivatives exhibit good inhibition properties in both acidic solutions, and the adsorption on the carbon steel surface follows the Langmuir isotherm model in both acidic media. Theoretical calculations were also performed, and the calculated quantum parameters correlated with the experimental results, thus supporting the conclusions reached from the electrochemical data.

---

**Keywords:** Mesoionic Salts; Polarization; EIS; Molecular Modeling; Acid Corrosion.

### 1. INTRODUCTION

Corrosion has been one of the greatest issues in industrial processes as it brings about significant material and financial losses. Industrial metal structures are constantly exposed to an environment that promotes corrosion; in addition, acid pickling and the cleaning of equipment in refineries that use acidic media promotes and speeds metal corrosion, thus affecting equipment operation and durability [1,2]. Organic inhibitors have been used as promising alternatives to prevent corrosion. These inhibitors are usually adsorbed on the metal surface forming a coordinate bond (chemical adsorption) or are adsorbed through an electrostatic interaction between the inhibitor and the metal (physical adsorption) [3]. These interactions lead to the formation of a film that reduces or prevents the contact of the metal surface with the corrosive medium. Several reports have shown that

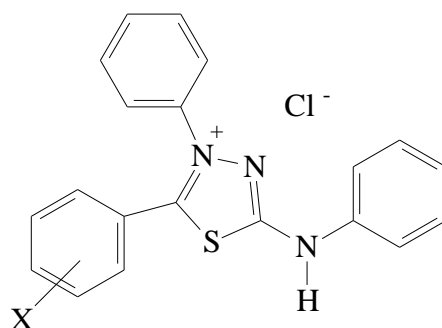
heterocyclic compounds containing nitrogen, oxygen and sulfur atoms have anticorrosion activity on carbon steel in acidic media [4,5]. The polar groups containing these atoms and electrons are usually adsorbed on the metal surface forming a uniform coating [6-11].

Although there are several studies in the literature regarding corrosion efficiency and heterocyclic compounds, the heterocyclic compounds containing a thiadiazolium ring have shown more significant efficiency on copper and steel in acidic and salt media [12-15] over others. Additionally, salts of the thiadiazolium class, named mesoionic compounds, have been little studied to date [16,17]. The corrosion inhibition efficiency of these compounds might be connected to the low values of ionization energy, which work as electron donors, besides the presence of nucleophilic and electrophilic centers in their structures, which promote the adsorption of the molecules on the metal surface. In addition, the presence of a sulfur atom favors a greater interaction when compared to other compounds with an oxygen atom [6,18,19].

Therefore, the aim of this work was to evaluate the inhibitory properties of four mesoionic compounds of the 1,3,4-thiadiazolium-2-phenylamine chloride, MI-1, MI-2, MI-3 and MI-4, on AISI 1020 carbon steel in HCl 1.0 mol L<sup>-1</sup> and in H<sub>2</sub>SO<sub>4</sub> 0.5 mol L<sup>-1</sup> using the electrochemical techniques of potentiodynamic polarization (PP), linear resistance to polarization (LRP) and electrochemical impedance spectroscopy (EIS). Further, density functional theory (DFT) calculations were performed, and the quantum parameters, HOMO (highest occupied molecular orbital) and LUMO (lowest unoccupied molecular orbital) energies, charges and hardness were used to correlate the structure of the 1,3,4-thiadiazolium-2-phenylamine salts with their corrosion inhibition efficiencies on carbon steel in HCl and H<sub>2</sub>SO<sub>4</sub> acids.

## 2. MATERIALS AND METHODS

### 2.1. Synthesis of 5-(X-phenyl)-1,3,4-thiadiazolium-2-phenylamine chloride (MI 1-4)



X = 4-Cl (MI-1); 4-F (MI-2); 2-Cl (MI-3); 2-F (MI-4)

**Figure 1.** Chemical structure of the mesoionic chlorides MI 1-4.

The mesoionic derivatives 5-(4' or 2'-X-phenyl)-1,3,4-thiadiazolium-2-phenylamine chloride (MI 1-4), where MI-1 X=4-Cl, MI-2 X=4-F, MI-3 X=2-Cl, and MI-4 X=2-F (Figure 1), were prepared

by convergent synthesis using 1,4-diphenyl-thiosemicarbazide, substituted benzaldehydes in the presence of  $\text{SOCl}_2$  and few drops of 1,4-dioxane for homogenization of the reaction mixture. Afterwards, the mixture was submitted to microwave irradiation in a scientific oven (CEM-Discover, magneton 2,450 MHz) [20]. The solids formed were placed in cold 1,4-dioxane and then were filtered and washed with cold hexane. All compounds were fully characterized by IR,  $^1\text{H}$  and  $^{13}\text{C}$  NMR methods.

*5-(4'-chloro-phenyl)-1,3,4-thiadiazolium-2-phenylamine chloride – MI-1*

Yield 52%, m.p. 262 °C. Infrared (KBr)  $\nu$   $\text{cm}^{-1}$ : 3429 (N-H), 3049 (C-H aromatic), 2849 ( $\text{C}=\text{N}^+$ ), 1570 (C=N), 1321 (C-S), 831 (C-Cl).  $^1\text{H}$  NMR (DMSO- $d_6$ )  $\delta$  (ppm): 12.93 (s, 1H, N-H), 7.94–7.43 (m, 14H, H-C), 7.15 (t, 1H, H-C4''').  $^{13}\text{C}$  NMR (DMSO- $d_6$ )  $\delta$  (ppm): 163.4 (C2), 161.2 (C5), 138.9 (C4'), 138.5 (C1'''), 138.0 (C1''), 122.6 (C1'). Anal. Calc. for  $\text{C}_{20}\text{H}_{15}\text{Cl}_2\text{N}_3\text{S}$ : C, 60.01; H, 3.78; N, 10.50; Found: C, 60.06; H, 3.82; N, 10.47.

*5-(4'-fluor-phenyl)-1,3,4-thiadiazolium-2-phenylamine chloride – MI-2*

Yield 75%, m.p. 208 °C. Infrared (KBr)  $\nu$   $\text{cm}^{-1}$ : 3435 (N-H), 3049 (C-H), 2774 ( $\text{C}=\text{N}^+$ ), 1572 (C=N), 1323 (C-F), 1138 (C-S).  $^1\text{H}$  NMR (DMSO- $d_6$ )  $\delta$  (ppm): 12.85 (s, 1H, N-H), 7.75–7.41 (m, 14H, H-C), 7.16 (t, 1H, H-C 4''').  $^{13}\text{C}$  NMR (DMSO- $d_6$ )  $\delta$  (ppm): 165.6 (C2), 163.6 (C4'), 160.8 (C5), 138.7 (C1'''), 138.8 (C1''), 119.9 (C1'). Anal. Calc. for  $\text{C}_{20}\text{H}_{15}\text{ClFN}_3\text{S}$ : C, 62.58; H, 3.90; N, 10.95; Found: C, 62.63; H, 3.96; N, 10.89.

*5-(2'-chloro-phenyl)-1,3,4-thiadiazolium-2-phenylamine chloride – MI-3*

Yield 80%, m.p. 258 °C. Infrared (KBr)  $\nu$   $\text{cm}^{-1}$ : 3431 (N-H), 3059 (C-H), 2689 ( $\text{C}=\text{N}^+$ ), 1568 (C=N), 762 (C-Cl), 689 (C-S).  $^1\text{H}$  NMR (DMSO- $d_6$ )  $\delta$  (ppm): 12.92 (s, 1H, N-H), 7.89–7.44 (m, 13H, H-C), 7.16 (t, 1H, C-H).  $^{13}\text{C}$  NMR (DMSO- $d_6$ )  $\delta$  (ppm): 162.8 (C2), 160.9 (C5), 138.8 (C1'''), 137.8 (C1''), 132.8 (C2'). Anal. Calc. for  $\text{C}_{20}\text{H}_{15}\text{Cl}_2\text{N}_3\text{S}$ : C, 60.01; H, 3.78; N, 10.50; Found: C, 60.07; H, 3.83; N, 10.44.

*5-(2'-fluor-phenyl)-1,3,4-thiadiazolium-2-phenylamine chloride – MI-4*

Yield 98%, m.p. 207 °C. Infrared (KBr)  $\nu$   $\text{cm}^{-1}$ : 3437 (N-H), 3057 (C-H), 2664 ( $\text{C}=\text{N}^+$ ), 1570 (C=N), 1323 (C-S), 1225 (C-F), 689 (C-S).  $^1\text{H}$  NMR (DMSO- $d_6$ )  $\delta$  (ppm): 12.97 (s, 1H, N-H), 7.68–7.35 (m, 13H, H-C), 7.14 (t, 1H, H-C 4''').  $^{13}\text{C}$  NMR (DMSO- $d_6$ )  $\delta$  (ppm): 161.9 (C2), 159.5 (C2'), 157.4 (C5), 138.4 (C1'''), 137.9 (C1'), 111.5 (C1'). Anal. Calc. for  $\text{C}_{20}\text{H}_{15}\text{ClFN}_3\text{S}$ : C, 62.58; H, 3.90; N, 10.95; Found: C, 62.61; H, 3.94; N, 10.91.

## 2.2. Theoretical calculations

Theoretical calculations were performed using density functional theory (DFT) with the M06-2X functional and 6-31+g (d,p) basis set. The functional and basis set were chosen based on previous studies. The M06-2X functional, a meta exchange-correlation functional [21], has been proven to be

very reliable for investigations on reaction mechanisms and has overcome the popular B3LYP functional in predicting quantitative structure-property relationships and local quantum descriptors [22]. Zhan and co-authors demonstrated that 6-31+g (d,p) is such an economical basis set that it is sufficient for predicting the energy of the frontier orbitals [23]. The geometry of each 1,3,4-thiadiazolium-2-phenylamine salt was optimized and confirmed by inspection of the vibrational frequencies calculated at the same level of theory. The energies of the frontier orbitals were determined from these calculations, as well as from several correlated quantities (HOMO-LUMO gap, hardness ( $\eta$ ) and ionization energy, the latter was obtained from Koopmans' theorem). The Mulliken charges on each atom and the molecule dipole moment ( $\mu$ ) were also determined.

### 2.3. Electrochemical experiments

Stock solutions were prepared in methanol: Milli-Q water (7:3 v/v) at concentrations of  $3.5 \times 10^{-9}$ ;  $1.75 \times 10^{-8}$  and  $3.5 \times 10^{-8}$  mol L<sup>-1</sup> in 1.0 mol L<sup>-1</sup> HCl and 0.5 mol L<sup>-1</sup> H<sub>2</sub>SO<sub>4</sub>.

Assays were performed at room temperature using an electrochemical three-electrode cell, paired with a working electrode of AISI 1020 carbon steel (a surface area of 0.786 cm<sup>2</sup>; composition (%): C: 0.17, P: 0.04, S: 0.05, Mn: 0.30; and the remainder in Fe), a platinum auxiliary electrode and a silver/ silver chloride (Ag/AgCl) reference electrode. The electrode was prepared by embedding the steel rods in epoxy resin and exposing the surface area. Before each measurement, the steel surface was abraded with 600, 800 and 1200 grade emery paper, washed with triply distilled water, degreased with ethanol and dried [24]. The electrolytes were 1 mol L<sup>-1</sup> HCl and 0.5 mol L<sup>-1</sup> H<sub>2</sub>SO<sub>4</sub>, and all experiments were carried out in 40 mL solutions of naturally aerated electrolyte at 25 °C.

Measurements were taken using Autolab PGstat potentiostat/galvanostat; PP and EIS data were analyzed using NOVA 1.8 software. PP measurements were performed at a 1 mV s<sup>-1</sup> scan rate with potential ranging at  $\pm 200$  mV around the open circle potential ( $E_{OCP}$ ) after the immersion of the working electrode for 30 min to reach steady-state conditions. EIS measurements were taken through the corrosion potential ( $E_{corr}$ ) in an interval between 0.1 and 100,000 Hz with a 10 mV peak-to-peak amplitude using an alternating current signal. In the LPR assays, the potentials ranged between -10 mV and +10 mV. The polarization resistance ( $R_p$ ) in carbon steel was obtained by the slope of the straight line, and this value was associated with the resistance to material corrosion.

## 3. RESULTS AND DISCUSSION

### 3.1. Synthesized compounds

The synthesized mesoionic salts (MI-1–MI-4) were obtained in good yields, and the chemical structures were confirmed using elemental analyses, FTIR, <sup>1</sup>H NMR and <sup>13</sup>C NMR spectroscopies as indicated in Materials and Methods.

### 3.2. Potentiodynamic Polarization measurements

Potentiodynamic polarization has enabled the evaluation of the anticorrosion activity based on the current density of each compound (MI – 1-4).

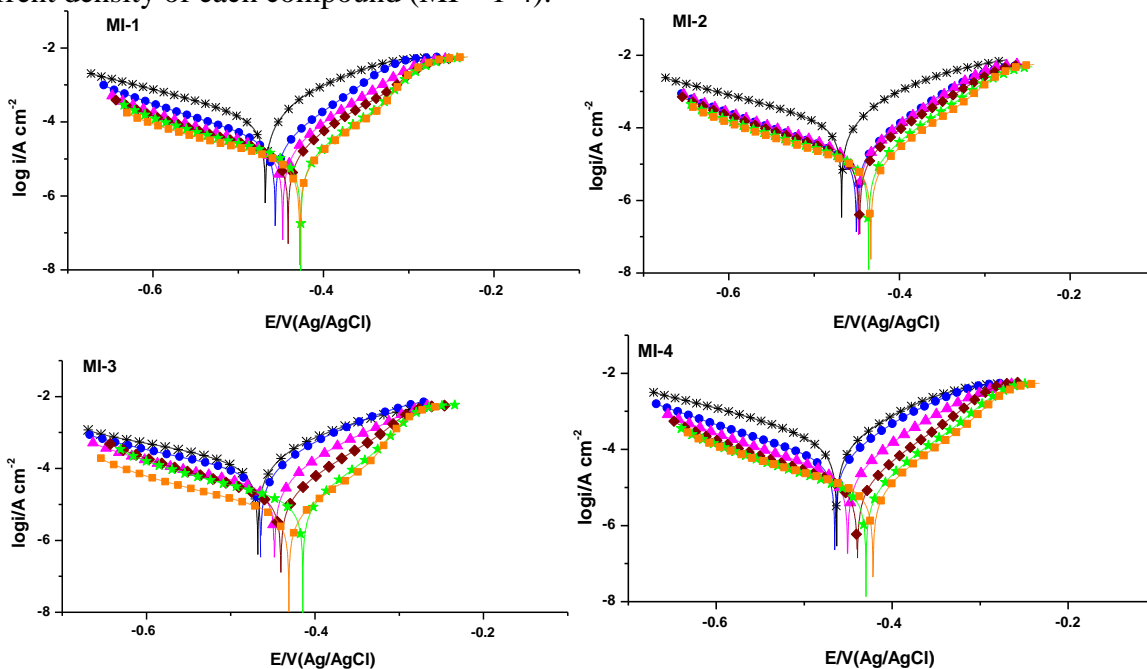


**Figure 2.** Polarization curves for AISI 1020 carbon steel in 1.0 mol L<sup>-1</sup> HCl, in the presence or absence of MI 1-4 at different concentrations: + Blank (without inhibitor); ● 3.15×10<sup>-5</sup> mol L<sup>-1</sup>; ▲ 9.4×10<sup>-5</sup> mol L<sup>-1</sup>; ◆ 1.5×10<sup>-4</sup> mol L<sup>-1</sup>; \* 2.5×10<sup>-4</sup> mol L<sup>-1</sup>; and ■ 3.15×10<sup>-4</sup> mol L<sup>-1</sup>.

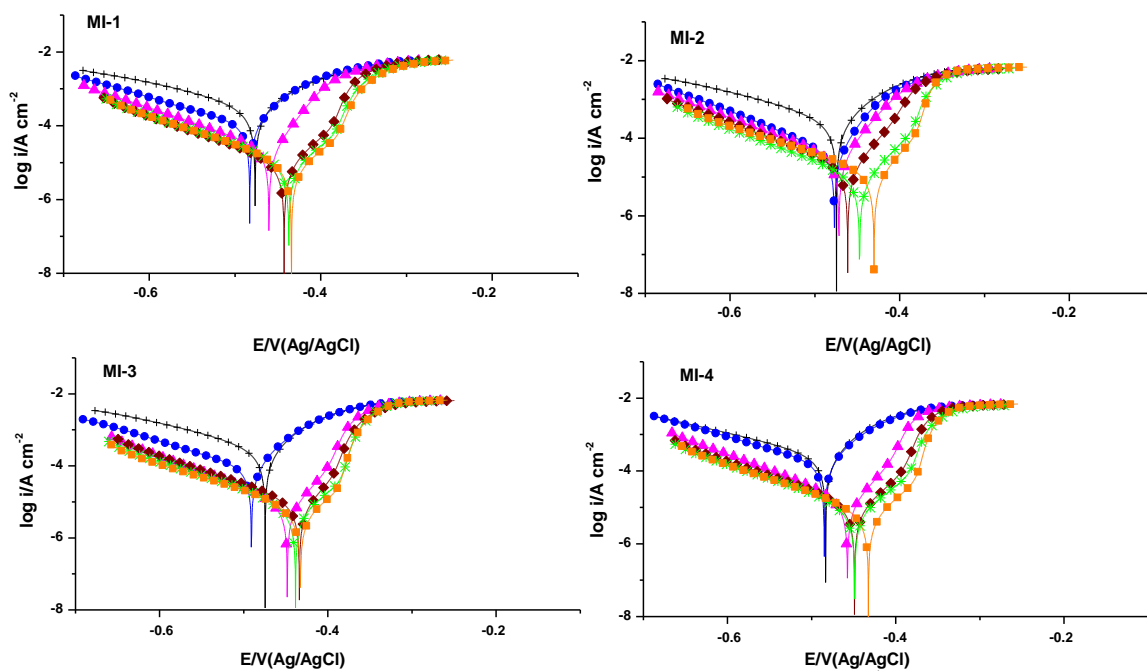


**Figure 3.** Polarization curves for AISI 1020 carbon steel in 0.5 mol L<sup>-1</sup> H<sub>2</sub>SO<sub>4</sub>, in the presence or absence of MI 1-4 at different concentrations: + Blank (without inhibitor); ● 3.15×10<sup>-5</sup> mol L<sup>-1</sup>; ▲ 9.4×10<sup>-5</sup> mol L<sup>-1</sup>; ◆ 1.5×10<sup>-4</sup> mol L<sup>-1</sup>; \* 2.5×10<sup>-4</sup> mol L<sup>-1</sup>; and ■ 3.15×10<sup>-4</sup> mol L<sup>-1</sup>.

Tafel curves were obtained using the data from these assays,  $\log i_{\text{corr}}$  versus the current potential (Figures 2 and 3). As shown in Figures 2 and 3, the values of the corrosion current density ( $i_{\text{corr}}$ ) decrease with the increasing concentration of the inhibitory compounds for both acids, HCl and H<sub>2</sub>SO<sub>4</sub>. The decline in the corrosion current density in the presence of the inhibitor may be associated with the adsorption of the mesoionic chlorides on the carbon steel surface.

According to the PP curves, the presence of the inhibitors promoted a reduction in the density of both the anodic and cathodic currents, as well as an  $E_{\text{corr}}$  shift in all tested compounds in both acids. These results indicated that by adding corrosion inhibitors to the solution, the steel anodic dissolution decreases, the cathodic evolution of hydrogen is delayed in both acids and such effects are increased with the increasing concentration of the inhibitors.

The linear resistance to polarization (LRP) tests were performed under the same conditions as the potentiodynamic polarization (PP) tests with MI 1-4 compounds and both acids. The inhibition efficiency was calculated using Equation 1.

$$\eta_{\text{LPR}}(\%) = \frac{R_p - R_p^0}{R_p} \times 100 \quad (1)$$

where  $R_p$  and  $R_p^0$  are the polarization resistance values in the presence and the absence of the inhibitor, respectively.

Tables 1 and 2 show the inhibition efficiency values for each concentration, as well as the kinetic electrochemical parameters, such as the corrosion potential ( $E_{\text{corr}}$ ), cathodic and anodic Tafel slopes ( $b_c$  and  $b_a$ ) and corrosion current density ( $j_{\text{corr}}$ ), obtained by the extrapolation of the Tafel lines, for AISI 1020 carbon steel in 1 mol L<sup>-1</sup> HCl and 0.5 mol L<sup>-1</sup> H<sub>2</sub>SO<sub>4</sub> solutions. The inhibition efficiencies ( $\eta_{\text{LPR}}$  %) by LRP for both acids are also shown in Tables 1 and 2.

**Table 1.** Kinetic parameters obtained from the Tafel plots and the anticorrosion efficiency obtained by the potentiodynamic polarization and linear polarization resistance ( $\eta_{\text{LPR}}$ ) for C-steel in 1 mol L<sup>-1</sup> HCl in the presence or absence of the mesoionic hydrochlorides (MI 1-4).

Inhibitor Concentration (mol L <sup>-1</sup> )	Potentiodynamic polarization-PP				LPR
	$\beta_a$ (mV dec <sup>-1</sup> )	$\beta_c$ (mV dec <sup>-1</sup> )	$E_{\text{corr}}$ (mV/SCE)	$j_{\text{corr}}$ (10 <sup>-5</sup> A cm <sup>-2</sup> )	$\eta_{\text{LPR}}$ (%)
Blank	0.2686	0.089303	-0.46792	0.00021	-
MI-1					
3.15×10 <sup>-5</sup>	0.1330	0.0635	-0.4551	2.61	73
9.4×10 <sup>-5</sup>	0.1826	0.0633	-0.4480	1.84	79
1.5×10 <sup>-4</sup>	0.1992	0.0699	-0.4416	1.64	84
2.5×10 <sup>-4</sup>	0.1928	0.0693	-0.4226	1.02	92
3.15×10 <sup>-4</sup>	0.1944	0.0687	-0.4263	0.92	91
MI-2					
3.15×10 <sup>-5</sup>	0.1239	0.0602	-0.4671	3.59	52
9.4×10 <sup>-5</sup>	0.1454	0.0616	-0.4517	2.09	67
1.5×10 <sup>-4</sup>	0.1575	0.0635	-0.4472	1.77	78

$2.5 \times 10^{-4}$	0.1675	0.0603	-0.4346	1.34	85
$3.15 \times 10^{-4}$	0.1645	0.0627	-0.4322	0.99	88
MI-3					
$3.15 \times 10^{-5}$	0.2798	0.0831	-0.4643	9.91	46
$9.4 \times 10^{-5}$	0.4847	0.0720	-0.4482	6.50	69
$1.5 \times 10^{-4}$	0.1779	0.0708	-0.4405	1.88	77
$2.5 \times 10^{-4}$	0.1538	0.0572	-0.4144	0.92	87
$3.15 \times 10^{-4}$	0.1578	0.0741	-0.4310	0.59	92
MI-4					
$3.15 \times 10^{-5}$	0.0839	0.1336	-0.4793	5.56	50
$9.4 \times 10^{-5}$	0.1608	0.0617	-0.4497	2.38	76
$1.5 \times 10^{-4}$	0.1426	0.0594	-0.4393	1.13	88
$2.5 \times 10^{-4}$	0.1559	0.0601	-0.4297	0.85	91
$3.15 \times 10^{-4}$	0.1719	0.0629	-0.4191	0.88	92

**Table 2.** Kinetic parameters obtained from the Tafel plots and anticorrosion efficiency obtained by the potentiodynamic polarization and linear polarization resistance ( $\eta_{LPR}$ ) for C-steel in 0.5 mol L<sup>-1</sup> H<sub>2</sub>SO<sub>4</sub> in the presence or absence of the mesoionic hydrochlorides (MI 1-4).

Inhibitor concentration (mol L <sup>-1</sup> )	Potentiodynamic polarization-PP				LPR
	$\beta_a$ (mV dec <sup>-1</sup> )	$\beta_c$ (mV dec <sup>-1</sup> )	$E_{corr}$ (mV/SCE)	$j_{corr}$ ( $10^{-5}$ A cm <sup>-2</sup> )	$\eta_{LPR}$ (%)
Blank	0.2377	0.1051	-0.4749	42.879	-
MI-1					
$3.15 \times 10^{-5}$	0.1813	0.0541	-0.4800	12.05	43
$9.4 \times 10^{-5}$	0.0928	0.0357	-0.4646	1.96	75
$1.5 \times 10^{-4}$	0.1147	0.0585	-0.4430	0.94	96
$2.5 \times 10^{-4}$	0.1092	0.0724	-0.4389	1.00	96
$3.15 \times 10^{-4}$	0.1137	0.0782	-0.4353	0.90	96
MI-2					
$3.15 \times 10^{-5}$	0.1286	0.0415	-0.4765	4.97	64
$9.4 \times 10^{-5}$	0.1460	0.0448	-0.4736	3.89	65
$1.5 \times 10^{-4}$	0.1093	0.0449	-0.4573	1.62	83
$2.5 \times 10^{-4}$	0.1200	0.0539	-0.4409	0.96	95
$3.15 \times 10^{-4}$	0.0919	0.0461	-0.4310	0.97	94
MI-3					
$3.15 \times 10^{-5}$	0.1550	0.0531	-0.4875	9.52	47
$9.4 \times 10^{-5}$	0.0534	0.0381	-0.4494	0.38	95
$1.5 \times 10^{-4}$	0.0485	0.0353	-0.4342	0.41	95
$2.5 \times 10^{-4}$	0.0684	0.0562	-0.4388	0.41	96
$3.15 \times 10^{-4}$	0.0903	0.0671	-0.4319	0.47	97
MI-4					

$3.15 \times 10^{-5}$	0.1064	0.0344	-0.4691	3.36	72
$9.4 \times 10^{-5}$	0.0509	0.0353	-0.4540	0.64	92
$1.5 \times 10^{-4}$	0.0680	0.0513	-0.4517	0.70	91
$2.5 \times 10^{-4}$	0.1046	0.0729	-0.4478	0.87	96
$3.15 \times 10^{-4}$	0.0744	0.0530	-0.4340	0.46	96

### 3.3. Electrochemical Impedance Spectroscopy (EIS)

EIS assays have confirmed the results obtained by the PP and LRP techniques. A Nyquist plot is an alternative way to represent the results at characteristic frequencies using the charge transfer function and varying the frequency from zero to infinity. The Nyquist plots in Figures 4 and 5 show a single semicircle shifted along the real impedance axis ( $Z_{real}$ ), thus indicating that the tested compounds exhibit anticorrosion efficiency controlled by a load transfer process for both HCl and  $H_2SO_4$  [25]. The inhibition efficiencies for each inhibitor concentration in both electrophilic media were calculated using Equation 2 [26].

$$\eta_{EIS}(\%) = \frac{R_{ct} - R_{ct}^0}{R_{ct}} \times 100 \tag{2}$$

The Nyquist plots showed a capacitive arc, since the carbon steel electrode generates a signal related to the formation of a passive film. The corrosion resistance can be determined through the Nyquist diagram. The less developed the arc in the diagram is, the larger the diameter of the semicircle extrapolated at the real axis ( $Z'$ ) is.

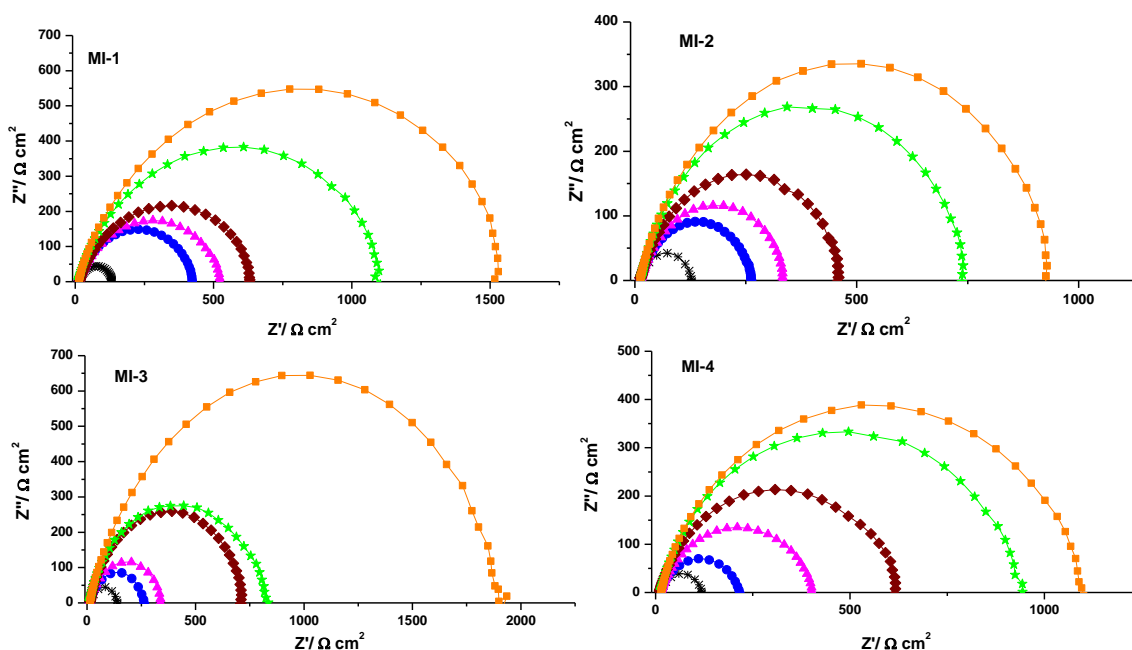


**Figure 4.** Nyquist diagrams for AISI 1020 carbon steel in 1.0 mol L<sup>-1</sup> HCl, in the presence or absence of MI1-4 at different concentrations: + Blank (without inhibitor); ●  $3.15 \times 10^{-5}$  mol L<sup>-1</sup>; ▲  $9.4 \times 10^{-5}$  mol L<sup>-1</sup>; ◆  $1.5 \times 10^{-4}$  mol L<sup>-1</sup>; \*  $2.5 \times 10^{-4}$  mol L<sup>-1</sup>; and ■  $3.15 \times 10^{-4}$  mol L<sup>-1</sup>.

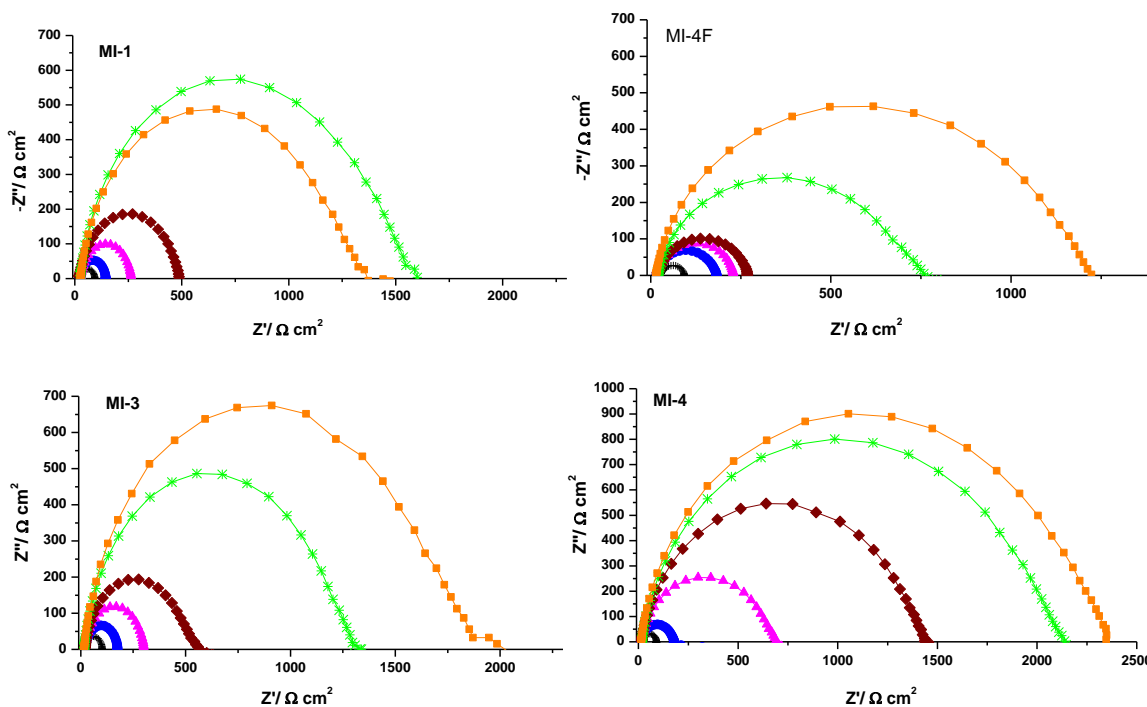


**Figure 5.** Nyquist diagrams for AISI 1020 carbon steel in 0.5 mol L<sup>-1</sup> H<sub>2</sub>SO<sub>4</sub>, in the presence or the absence of MI 1-4 at different concentrations: + Blank (without inhibitor); ● 3.15×10<sup>-5</sup> mol L<sup>-1</sup>; ▲ 9.4×10<sup>-5</sup> mol L<sup>-1</sup>; ◆ 1.5×10<sup>-4</sup> mol L<sup>-1</sup>; \* 2.5×10<sup>-4</sup> mol L<sup>-1</sup>; and ■ 3.15×10<sup>-4</sup> mol L<sup>-1</sup>.

MI-3 demonstrated the best corrosion inhibition efficiency at a concentration of 3.5×10<sup>-8</sup> mol L<sup>-1</sup>, i.e., 92% by EIS and 93% by LRP in the presence of HCl and 99% by EIS and 97% by LRP in the presence of H<sub>2</sub>SO<sub>4</sub>. The interaction between the inhibitor and the metal surface did not show a significant change after the positioning of the substituent chlorine in the aromatic ring. Although there have been no reports in the literature regarding the anticorrosion efficiency of salts derived from the 1,3,4-thiadiazolium-2-phenylamines, other heterocyclic compounds from the 1,3,4-thiadiazole class showed good efficiencies in a HCl medium on mild steel at lower concentrations. For instance, at a concentration of 12×10<sup>-4</sup> mol L<sup>-1</sup>, 2,5-bis-(3-pyridyl)-1,3,4-thiadiazole presented efficiencies of 93.5% and 98% by PP and EIS in HCl and 91% and 96.7% in H<sub>2</sub>SO<sub>4</sub>, respectively [27]. However, at a concentration of 6×10<sup>-3</sup> mol L<sup>-1</sup>, 4-amino-5-phenyl-1,3,4-thiadiazole showed efficiencies of 77.6% and 88.6% by PP and EIS in HCl and 95.8% and 96.6% in H<sub>2</sub>SO<sub>4</sub>, respectively [28]. Finally, at a concentration of 12×10<sup>-4</sup> mol L<sup>-1</sup>, 2,5-bis-(4-pyridyl)-1,3,4-thiadiazole presented efficiencies of 85.8% and 86.6% by PP and EIS in HCl and 82.6% and 82.3% in H<sub>2</sub>SO<sub>4</sub>, respectively [29].

The double-layer capacitance (*C<sub>dl</sub>*), which provides information on the protective film formed on the metal surface using Equation 3, was calculated through the electrochemical impedance. Tables 3 and 4 show the values used for calculating the double-layer capacitance in HCl and H<sub>2</sub>SO<sub>4</sub> assays, respectively.

$$C_{dl} = \frac{1}{2\pi f_{max} R_{ct}} \tag{3}$$

where  $f_{max}$  is the frequency in which the imaginary component shows the maximum frequency and  $R_{ct}$  is the charge transfer resistance.

Figure 6 illustrates the equivalent circuit used for the analysis of all EIS spectra in both acids, thus representing a single charge transfer reaction, which corroborates the experimental results [30-33].

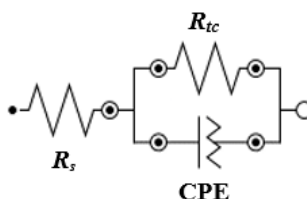


**Figure 6.** Equivalent circuit model used to fit the EIS experimental data.

Tables 3 and 4 show the values of the EIS parameters: solution resistance ( $R_s$ ), charge transfer resistance ( $R_{ct}$ ), double-layer capacitance ( $C_{dl}$ ), inhibition efficiency ( $\eta$  %) and the degree of surface coverage ( $\theta$ ).

**Table 3.** Electrochemical parameters obtained from the EIS plots for C-steel in 1 mol L<sup>-1</sup> HCl in the presence or absence of the mesoionic hydrochlorides (MI 1-4).

Inhibitor concentration (mol L <sup>-1</sup> )	$\theta$	$R_{ct}$ ( $\Omega$ cm <sup>2</sup> )	$f_{max}$ (Hz)	$C_{dl}$ ( $\mu$ F cm <sup>-2</sup> )	$\eta_{EIS}$ (%)
Blank	-	44.73	-	25.6	-
MI-1					
3.15×10 <sup>-5</sup>	0.69	148.91	7.94	46.61	69
9.4×10 <sup>-5</sup>	0.75	174.28	7.94	37.53	75
1.5×10 <sup>-4</sup>	0.79	216.15	6.31	37.12	79
2.5×10 <sup>-4</sup>	0.88	383.00	3.98	31.64	88
3.15×10 <sup>-4</sup>	0.91	547.83	5.01	20.33	91
MI-2					
3.15×10 <sup>-5</sup>	0.51	90.82	15.84	47.98	51
9.4×10 <sup>-5</sup>	0.62	115.93	15.84	41.21	62
1.5×10 <sup>-4</sup>	0.72	163.87	12.59	26.01	72
2.5×10 <sup>-4</sup>	0.83	268.70	12.59	19.54	83
3.15×10 <sup>-4</sup>	0.86	335.15	7.94	19.66	86
MI-3					
3.15×10 <sup>-5</sup>	0.55	97.26	7.94	64.17	44
9.4×10 <sup>-5</sup>	0.63	122.25	12.59	31.99	63
1.5×10 <sup>-4</sup>	0.80	259.56	10.00	31.29	80
2.5×10 <sup>-4</sup>	0.87	336.71	6.31	28.36	87

$3.15 \times 10^{-4}$	0.92	644.23	5.01	15.28	93
MI-4					
$3.15 \times 10^{-5}$	0.45	69.40	12.59	55.94	45
$9.4 \times 10^{-5}$	0.71	134.97	10.00	41.37	71
$1.5 \times 10^{-4}$	0.81	213.30	10.00	26.87	81
$2.5 \times 10^{-4}$	0.87	333.37	7.94	20.61	87
$3.15 \times 10^{-4}$	0.90	395.82	6.31	20.85	90

**Table 4.** Electrochemical parameters obtained from the EIS plots for C-steel in  $0.5 \text{ mol L}^{-1} \text{ H}_2\text{SO}_4$  in the presence or the absence of the mesoionic hydrochlorides (MI 1-4).

Inhibitor concentration ( $\text{mol L}^{-1}$ )	$\theta$	$R_{ct}$ ( $\Omega \text{ cm}^2$ )	$f_{\text{máx}}$ (Hz)	$C_{dl}$ ( $\mu\text{F cm}^{-2}$ )	$\eta_{\text{EIS}}$ (%)
Blank	-	92.76	39.81	4.31	-
MI-1					
$3.15 \times 10^{-5}$	0.36	144.25	30.20	3.65	35
$9.4 \times 10^{-5}$	0.65	262.71	22.91	2.65	65
$1.5 \times 10^{-4}$	0.81	486.40	13.18	2.48	81
$2.5 \times 10^{-4}$	0.94	1588.27	5.75	0.17	94
$3.15 \times 10^{-4}$	0.93	1441.39	5.75	0.19	93
MI-2					
$3.15 \times 10^{-5}$	0.44	182.74	39.81	2.19	44
$9.4 \times 10^{-5}$	0.56	229.32	22.91	3.03	56
$1.5 \times 10^{-4}$	0.62	549.68	22.91	1.26	62
$2.5 \times 10^{-4}$	0.87	2048.84	13.18	0.59	87
$3.15 \times 10^{-4}$	0.92	1656.79	10.00	0.96	92
MI-3					
$3.15 \times 10^{-5}$	0.42	174.44	30.20	3.02	42
$9.4 \times 10^{-5}$	0.66	300.29	22.91	2.31	66
$1.5 \times 10^{-4}$	0.82	566.54	17.38	1.62	82
$2.5 \times 10^{-4}$	0.92	1332.70	13.18	0.91	92
$3.15 \times 10^{-4}$	0.95	1946.52	7.58	0.11	95
MI-4					
$3.15 \times 10^{-5}$	0.50	178.91	39.81	2.24	50
$9.4 \times 10^{-5}$	0.87	689.64	17.38	1.33	87
$1.5 \times 10^{-4}$	0.94	1435.90	10.00	1.11	94
$2.5 \times 10^{-4}$	0.96	2123.43	7.59	0.10	96
$3.15 \times 10^{-4}$	0.96	2349.30	7.59	0.09	96

As shown in Tables 3 and 4, the increase in the inhibitor concentration causes a rise in  $R_{ct}$  and a decrease in  $C_{dl}$  in both acids. These results might be connected to the higher adsorption of the inhibitors on the metal surface and at the interface with the solution. Therefore, the mechanism of corrosion inhibition involved in the mesoionic chlorides must be associated with a chemical adsorption since besides nitrogen (N), sulfur (S) is a soft atom with great polarizability, thus easily donating its free electrons from its  $d$  orbital to the  $d$  orbital of the metal (Fe), creating a strong inhibitor-metal interaction, hence forming a protective film adhered to the metal surface [34]. This hypothesis corroborates with the results obtained by the PP and LRP techniques, which presented inhibition efficiencies ranging from 83% to 93% at a concentration of  $3.5 \times 10^{-8}$  mol L<sup>-1</sup> in HCl, and from 94% to 95% in H<sub>2</sub>SO<sub>4</sub>. Further, in accord with the literature [27,29], the inhibition efficiency increased with inhibitor concentration, but the best performance was exhibited at the lower concentration in this study, namely,  $3.5 \times 10^{-8}$  mol L<sup>-1</sup>, when compared to  $12 \times 10^{-4}$  mol L<sup>-1</sup> with 85.8% and 82.3% for HCl and H<sub>2</sub>SO<sub>4</sub>, respectively, for 2,5-bis-(*n*-pyridyl)-1,3,4-thiadiazole [29].

Bode diagrams of the compounds evaluated in HCL and H<sub>2</sub>SO<sub>4</sub> are presented in Figures 7 and 8 and confirmed the performance observed in the Nyquist plots.

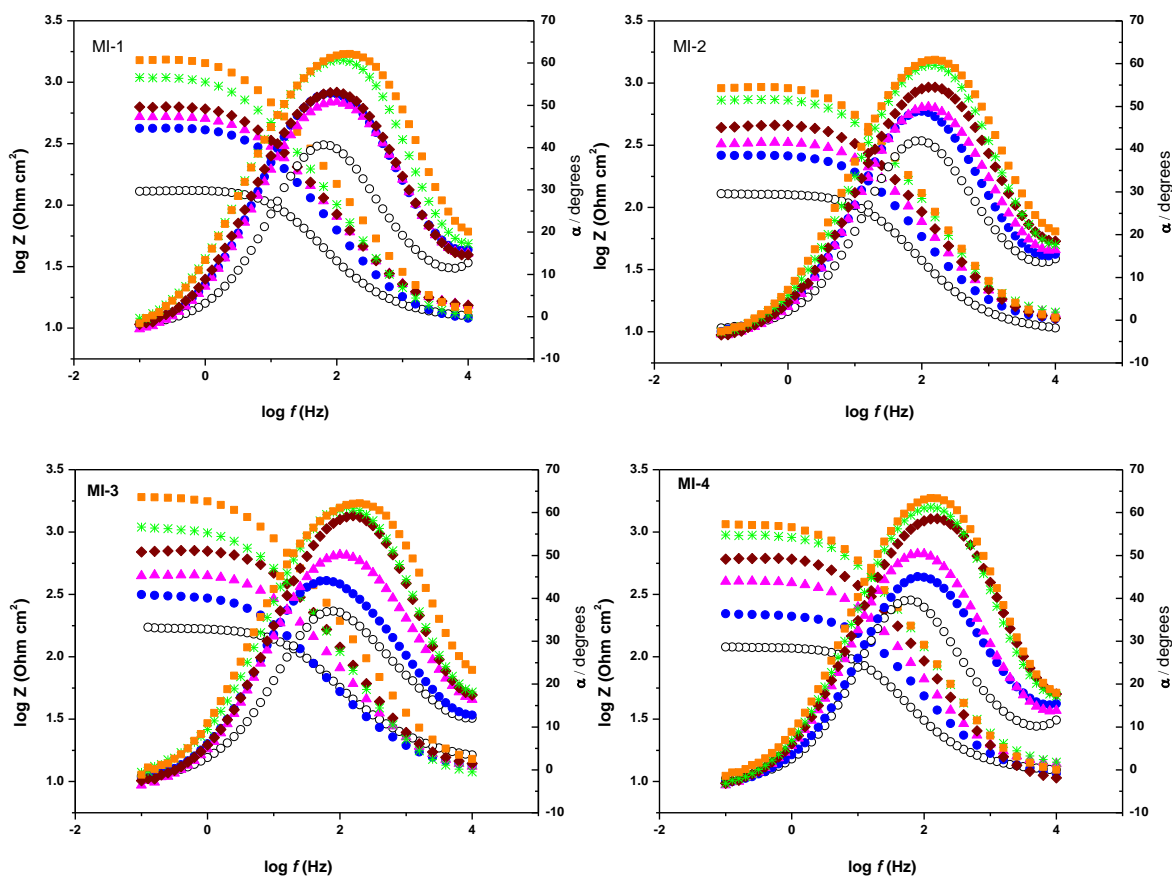


**Figure 7.** Bode plots for AISI 1020 carbon steel in 1.0 mol L<sup>-1</sup> HCl, in the presence or the absence of MI 1-4 at different concentrations: ○Blank (without inhibitor); ● $3.15 \times 10^{-5}$  mol L<sup>-1</sup>; ▲ $9.4 \times 10^{-5}$  mol L<sup>-1</sup>; ◆ $1.5 \times 10^{-4}$  mol L<sup>-1</sup>; \* $2.5 \times 10^{-4}$  mol L<sup>-1</sup>; and ■  $3.15 \times 10^{-4}$  mol L<sup>-1</sup>.

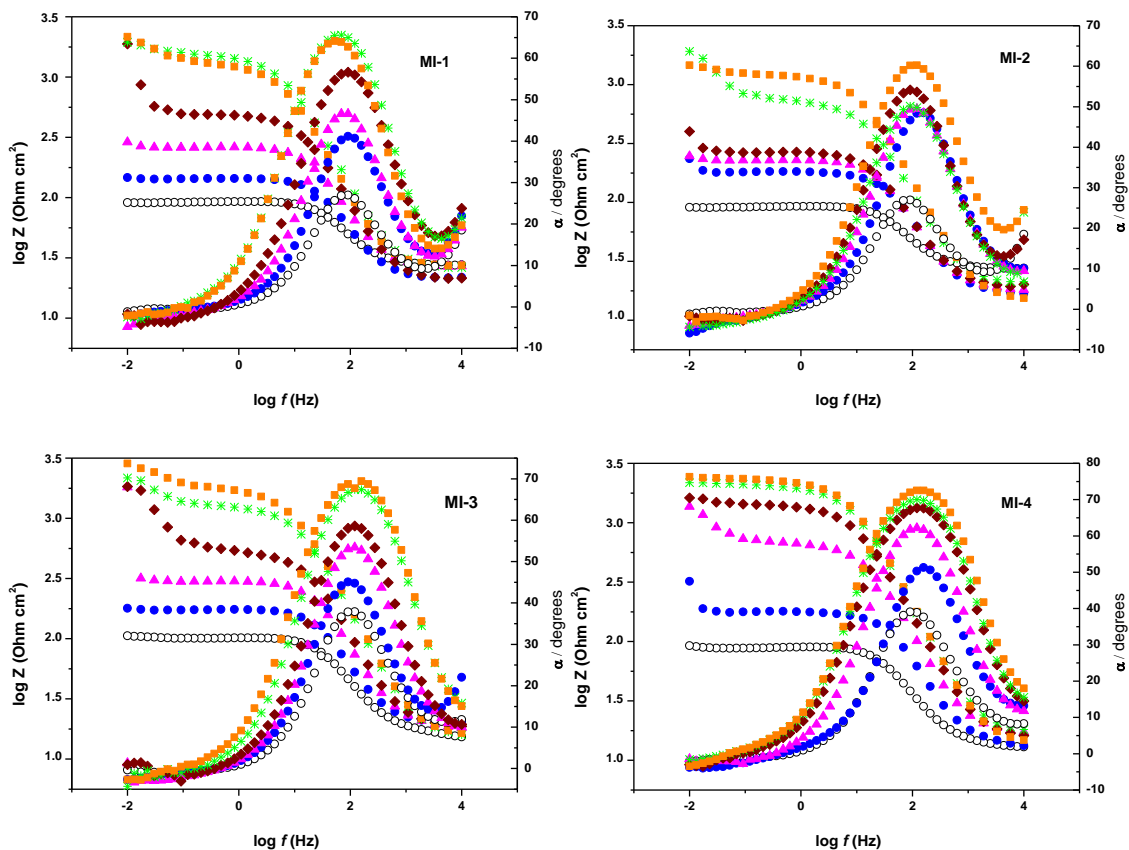


**Figure 8.** Bode plots for AISI 1020 carbon steel in 0.5 mol L<sup>-1</sup> H<sub>2</sub>SO<sub>4</sub>, in the presence or the absence of MI1-4 at different concentrations: ○Blank (without inhibitor); ●3.15×10<sup>-5</sup> mol L<sup>-1</sup>; ▲9.4×10<sup>-5</sup> mol L<sup>-1</sup>; ◆1.5×10<sup>-4</sup> mol L<sup>-1</sup>; \*2.5×10<sup>-4</sup> mol L<sup>-1</sup>; and ■ 3.15×10<sup>-4</sup> mol L<sup>-1</sup>.

The increase in log |Z| indicates better corrosion inhibition performance [35], and as seen in Figures 7 and 8, when the concentration of all assayed compounds increased, so did log |Z|. This finding indicates a capacitive behavior at high frequencies and an inductive behavior at low frequencies [36].

### 3.4. Adsorption isotherm

Corrosion inhibition depends on the ability of the inhibitors to adsorb on metal surfaces, and this information could be obtained through adsorption isotherms [9,36]. To obtain the adsorption isotherms, the degree of surface coverage of the inhibitor ( $\theta$ ) was calculated by EIS using Equation 4 [37].

$$\theta = \frac{R_{ct} - R_{ct}^0}{R_{ct}} \tag{4}$$

where  $R_{ct}$  and  $R_{ct}^0$  are the polarization resistance with and without the inhibitor, respectively.

The  $\theta$  values were tested graphically by fitting the different adsorption isotherms using the Temkin, Frumkin and Langmuir models. The Langmuir adsorption isotherm presented the best correlation coefficient (r) for all compounds tested in HCl. This isotherm is described by Equation 5

[35]. Under similar assayed conditions, reports in the literature that have involved derivatives containing the 1,3,4-thiadiazole ring have shown that they follow the Langmuir isotherm [27-29].

$$\frac{C_{inh}}{\theta} = \frac{1}{K_{ads}} + C_{inh} \quad (5)$$

where  $C_{inh}$  is the inhibitor concentration,  $\theta$  is the degree of surface coverage and  $K_{ads}$  is the adsorption equilibrium constant.

A good linear correlation coefficient was observed with the Langmuir isotherm in the  $H_2SO_4$  medium; the slope values were obtained in the range of 0.85-0.95, thus showing possible intermolecular interaction among the thiadiazolium salts. The modified Langmuir isotherm was then applied, as given by Equation 6 [38-40].

$$\frac{C_{inh}}{\theta} = \frac{n}{K_{ads}} + nC_{inh} \quad (6)$$

where  $n$  is a constant.

The standard free energy of adsorption ( $\Delta G_{ads}^0$ ) values were obtained using Equation 7, where  $R$  is the universal gas constant ( $J K^{-1} mol^{-1}$ ),  $T$  is the temperature (K), and 55.55 is the molar concentration ( $mol L^{-1}$ ) of water in the solution.

$$\Delta G_{ads}^0 = -RT \ln(55.55 K_{ads}) \quad (7)$$

Figure 9 shows the plot of  $C_{inh}/\theta$  versus  $C_{inh}$  indicating that straight lines were obtained for all mesoionic derivatives in  $1 mol L^{-1}$  HCl and  $H_2SO_4$  solutions, following the Langmuir and the modified Langmuir adsorption isotherms [27,38-40].

The high  $K_{ads}$  values for MI 1-4 indicate a strong interaction with the carbon steel surface, which can be attributed to the presence of a heterocycle containing nitrogen and sulfur atoms, as well as to the high  $\pi$ -electron shift between the aromatic rings and the thiadiazolium ring, in each of the studied compounds to the metal surface. Table 5 listed the thermodynamic parameters obtained. The  $\Delta G_{ads}^0$  values obtained in this study for the HCl solution range from -34.21 to -35.65  $kJ mol^{-1}$  and from -33.90 to -36.36  $kJ mol^{-1}$  in the  $H_2SO_4$  solutions. The negative values suggest that the adsorption mechanism of these compounds onto the AISI 1020 carbon steel surface in HCl and  $H_2SO_4$  media is a spontaneous process and that the adsorbed layer is stable. The results show that MI 1-4 were strongly adsorbed on the steel surface in both media. In fact, the positively charged nitrogen atoms of heterocyclic ring and the negatively charged carbon steel enable an electrostatic interaction promoting the adsorption process. This behavior is in accordance with the findings of other 1,3,4-thiadiazole compounds [27,28].

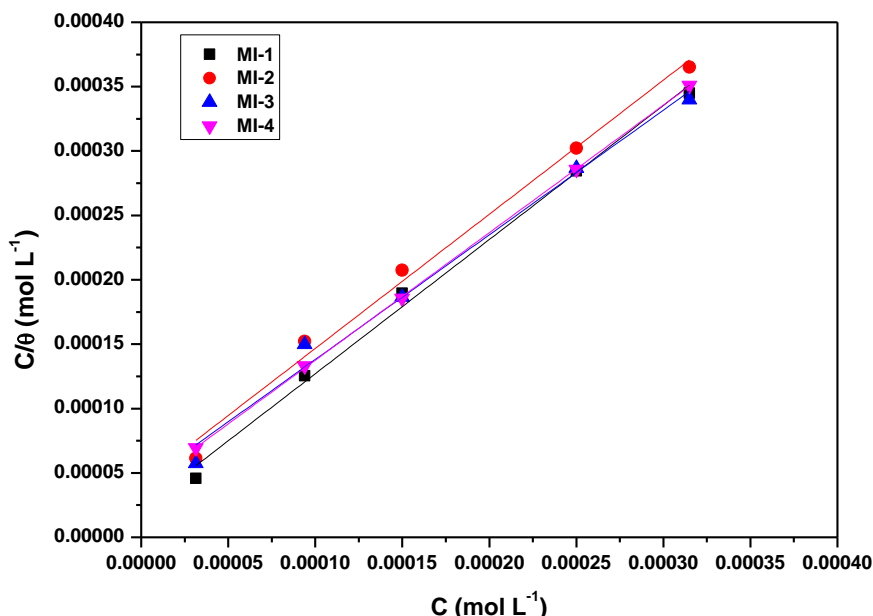


**Figure 9.** Langmuir isotherm plots for the adsorption of inhibitors on a C-steel surface in the presence of 1.0 mol L<sup>-1</sup> HCl.

**Table 5.** Thermodynamic parameters for the adsorption of mesoionic hydrochlorides (MI 1-4) in 1.0 mol L<sup>-1</sup> HCl on a carbon steel surface.

Compound	HCl <sup>a</sup> (1.0 mol L <sup>-1</sup> )				H <sub>2</sub> SO <sub>4</sub> <sup>b</sup> (0.5 mol L <sup>-1</sup> )				
	r <sup>c</sup>	slope	K <sub>ads</sub> (10 <sup>4</sup> L mol <sup>-1</sup> )	ΔG <sup>0</sup> <sub>ads</sub> (kJ mol <sup>-1</sup> )	r <sup>c</sup>	slope	n	K <sub>ads</sub> (10 <sup>4</sup> L mol <sup>-1</sup> )	ΔG <sup>0</sup> <sub>ads</sub> (kJ mol <sup>-1</sup> )
MI-1	0.994	1.04	2.77	-35.29	0.998	0.85	1.18	1.94	-34.40
MI-2	0.989	1.04	1.79	-34.21	0.973	0.90	1.11	1.56	-33.90
MI-3	0.985	0.97	3.20	-35.65	0.999	0.89	1.12	2.19	-34.72
MI-4	0.999	0.99	2.82	-35.34	0.998	0.95	1.05	4.29	-36.36

<sup>a</sup>Langmuir isotherm model; <sup>b</sup> modified Langmuir isotherm; <sup>c</sup> linear correlation coefficient.

### 3.5. Molecular modeling

Theoretical studies of corrosion inhibitor agents have been extensively used for correlating with experimental results [41]. In this work, the physicochemical properties of the mesoionic derivatives, such as the energy of the highest occupied molecular orbital ( $E_{HOMO}$ ) and the energy of the lowest unoccupied molecular orbital ( $E_{LUMO}$ ), as well as the dipole moment ( $\mu$ ), were calculated at the M06-2X/6-31+G (d,p) level. The HOMO-LUMO gap ( $\Delta E_{LUMO-HOMO}$ ) is relevant information, which generally correlates with the predicted corrosion inhibition, and the potential of corrosion inhibition increases as the  $\Delta E_{LUMO-HOMO}$  decreases [42]. Not only can effective corrosion inhibitors donate electrons to the vacant  $d$  orbitals of the metal to form a coordinate covalent bond but these inhibitors can also receive free electrons from the metal surface [43]. The higher the HOMO energy of the inhibitor is, the easier the donation of electrons to the unoccupied  $d$  orbitals of the metal is. While the lower the LUMO energy of the inhibitor is, the easier the reception of electrons from the metal is.

Thus, lower energy differences between HOMO and LUMO ( $\Delta E$ ) correspond to the greater potential for corrosion inhibition [44].

Table 6 shows the resulting values obtained for  $E_{\text{HOMO}}$ ,  $E_{\text{LUMO}}$ ,  $\Delta E_{\text{LUMO-HOMO}}$ , ionization energy and dipole moment calculated for the mesoionic derivatives (MI 1-4).

**Table 6.** Quantum properties calculated at the M06-2X/6-31+G (d,p) level:  $E_{\text{HOMO}}$  and  $E_{\text{LUMO}}$  (in Hartrees),  $\Delta E$ , hardness and ionization energies (in eV), Mulliken charge on the sulfur atom and dipole moment (in Debye).

	$E_{\text{HOMO}}$	$E_{\text{LUMO}}$	$\Delta E$	Hardness	Ionization Energy	Charge on S	Dipole Moment
	(Hartrees)			(eV)			(D)
MI-1	-0.40141	-0.18402	5.92	10.92	2.96	0.801	3.0427
MI-2	-0.40108	-0.18185	5.97	10.91	2.98	0.794	1.9421
MI-3	-0.41205	-0.17345	6.49	11.21	3.25	1.016	1.9693
MI-4	-0.40216	-0.1837	5.94	10.94	2.97	0.793	1.8397

The orbital energy values,  $E_{\text{HOMO}}$  and  $E_{\text{LUMO}}$ , calculated for all the molecules did not exhibit significant differences in the resulting band gap,  $\Delta E$ , hardness or ionization energies. Further, when analyzing the Mulliken charges of the atoms, the highest positive charge could be observed on the sulfur atom. The sulfur atom must exert a stronger interaction on the surface of the metals and can accept electrons from the  $d$  orbital of the iron to form a feedback bond; thus, the 1,3,4-thiadiazolium ring could adsorb on the Fe surface in a planar manner [28,45]. In fact, it is noticeable that the inhibition efficiency is slightly more sensitive to the charge on the sulfur atom than to the parameters related to the  $\Delta E$  values. The dipole moment represented a minor contribution to the inhibitor efficiency; even though these results correlate with the small differences observed in the corrosion inhibition efficiency in both acids.

#### 4. CONCLUSIONS

The mesoionic salts (MI 1-4) inhibit the corrosion of mild steel in HCl and H<sub>2</sub>SO<sub>4</sub> media, but the best performance was observed in 0.5 mol L<sup>-1</sup> H<sub>2</sub>SO<sub>4</sub>. The reason for the difference in inhibiting efficiency may be due to the competition between the inhibitor agents and anions, Cl<sup>-</sup> and SO<sub>4</sub><sup>2-</sup>, to get adsorbed onto the carbon steel surface. In HCl, the decrease in efficiency may be due to the protonation of the inhibitor agents, and these species have been adsorbed electrostatically with chloride ions on the carbon steel surface.

The compounds present a high corrosion efficiency as a mixed-type inhibitor for AISI 1020 carbon steel in 1 mol L<sup>-1</sup> HCl and 0.5 mol L<sup>-1</sup> H<sub>2</sub>SO<sub>4</sub>. Inhibition efficiencies increase by increasing the inhibitor concentration in both acids. The adsorption of MI 1-4 on the steel surface in HCl and H<sub>2</sub>SO<sub>4</sub> media follows the Langmuir and modified Langmuir isotherms, respectively, thus indicating that the main inhibition process occurs through adsorption. The theoretical parameters from the molecular modeling results revealed that the best inhibitor efficiency cannot be associated with the gap  $\Delta E_{\text{LUMO-HOMO}}$  values because of their small difference.

## ACKNOWLEDGMENTS

The authors thank CNPq (Conselho Nacional de Desenvolvimento Científico e Tecnológico), CAPES (Coordenação de Aperfeiçoamento de Pessoal de Nível Superior), and PETROBRAS (Petróleo Brasileiro) for financial support and fellowship.

## References

1. P.A. Schweitzer, *Fundamentals of Corrosion: Mechanisms, Causes, and Preventative Methods (Corrosion Technology)*, 1<sup>st</sup> edition, CRC Press, 2009.
2. A.S. Abdul Nabi and A.A. Hussain, *J. Basrah Res. (Sciences)*, 38 (2012) 125.
3. J. Tymoczko, W. Schuhmann and A.S. Bandarenka, *Electrochem. Comm.*, 27 (2013) 42.
4. N. Yilmaz, A. Fitoz, Ü. Ergun, and K.C. Emregül, *Corros. Sc.*, 111 (2016) 110.
5. A. Zarrouk, B. Hammouti, T. Lakhlifi, M. Traisnel, H. Vezin and F. Bentiss, *Corros. Sci.*, 90 (2015) 572.
6. C.M. Goulart, A. Esteves-Souza, C.A. Martinez-Huitle, C.J.F. Rodrigues, M.A.M. Maciel and A. Echevarria, *Corros. Sci.*, 67 (2013) 281.
7. E.A. Noor, *Corros. Sci.*, 47 (2005) 33.
8. G. Avci, *Mater. Chem. Phys.*, 112 (2008) 234.
9. S.K. Shukla and M.A. Quraishi, *Corros. Sci.*, 51 (2009) 1007.
10. E.C.M. Moura, A.D.N Souza, C.G.F.T. Rossi, D.R. Silva, M.A.M. Maciel, A. Echevarria and M.S.S. Bellieny, *Quim. Nova*, 36 (2013) 59.
11. F.S. de Souza and A. Spinelli, *Corros. Sci.*, 51 (2009) 642.
12. T.T. Qin, J. Li, H.Q. Luo, M. Li and N.B. Li, *Corros. Sci.*, 53 (2011) 1072.
13. W. Chen, S. Hong, H. Bing Li, H. Qun Luo, M. Li and N. Bing Li, *Corros. Sci.*, 61 (2012) 53.
14. M. Palomar-Pardavé, M. Romero-Romo, H. Herrera-Hernández, M.A. Abreu-Quijano, N.V. Likhanova, J. Uruchurtu and J.M. Juárez-García, *Corros. Sci.*, 54 (2012) 231.
15. F. Bentiss, B. Mernari, M. Traisnel, H. Vezin and M. Lagrenée, *Corros. Sci.*, 53 (2011) 487.
16. J. Vošta and J. Eliášek, *Werkst. Korros.*, 6 (1972) 487.
17. J.D. Cunha, C.G.F.T. Rossi, D.R. Silva, E.R.F. Teixeira, A. Echevarria and M.A.M. Maciel, Electrochemical study of 1,3,4-triazolium-2-thiol as corrosion inhibitor of mild steel in saline medium, in: E. Hart (Ed.), *Corrosion Inhibitors: Principles, Mechanisms and Applications*, chapter 6, Nova Science Publishers Inc., New York, USA, 2016.
18. T. Poornima, J. Nayak and A.N. Shetty, *Corros. Sci.*, 53 (2011) 3688.
19. E.M. Sherif and S.M. Park, *Corros. Sci.*, 48 (2006) 4065.
20. C.M. dos Reis, J. Echevarria-Lima, A.F. Miranda and A. Echevarria, *J. Braz. Chem. Soc.*, 22 (2011) 1505.
21. Y. Zhao and D.G. Truhlar, *Theor. Chem. Acc.*, 120 (2008) 215.
22. C.E. Rodrigues-Santos, A. Echevarria, C.M.R. Sant'Anna, T.B. Bitencourt, M.G. Nascimento and G.F. Bauerfeldt, *Molecules*, 20(2015) 17493.
23. C.-G. Zahn, J.A. Nichols and D.A. Dixon, *J. Phys. Chem. A*, 107 (2003) 4184.
24. M.A. Albuquerque, M.C.C. de Oliveira and A. Echevarria, *Int. Electrochem. Sci.*, 12 (2017) 852.
25. K.F. Khaled, *Appl. Surf. Sci.*, 255 (2008) 1811.
26. M.A. Sudheer and Quraishi, *Corros. Sci.*, 70 (2013) 161.
27. F. Bentiss, M. Lebrini, H. Vezin and M. Lagrenée, *Mater. Chem. Phys.*, 87 (2004) 18.
28. Y. Tang, X. Yang, W. Yang, Y. Chen and R. Wan, *Corr. Sci.*, 52 (2010) 242.
29. M. Lebrini, F. Bentiss, H. Vezin and M. Lagrenée, *Corros. Sci.*, 48 (2006) 1279.
30. L. Sadowski, *Arch. Civ. Mech. Eng.* 10 (2010) 109.

31. M. Behpour, S.M. Ghoreishi, N. Mohammadi, N. Soltani and M. Salavati-Niasari, *Corros. Sci.*, 52 (2010) 4046.
32. A.R. Hosein Zadeh, I. Danaee and M.H. Maddahy, *J. Mater. Sci. Technol.*, 29 (2013) 884.
33. G. Gao and C. Liang, *Electrochim. Acta*, 52 (2007) 4554.
34. W.H. Li, Q. He, S.T. Zhang, C.L. Pei and B.R. Hou, *J. Appl. Electrochem.*, 38 (2008) 289.
35. L.A. Al Juhaiman, *Int. J. Electrochem. Sci.*, 11 (2016) 2247.
36. D. Ozkır, K. Kayakırılmaz, E. Bayol, A.A. Gurten and F. Kandemirli, *Corros. Sci.*, 56 (2012) 143.
37. M. Lebrini, F. Robert, H. Vezin and C. Roos, *Corros. Sci.*, 52 (2010) 3367.
38. R.V.F. Villamil, P. Corio, J.C. Rubim and S.M.L. Agostinho, *J. Electroanal. Chem.*, 472 (1999) 112.
39. R.V.F. Villamil, P. Corio, J.C. Rubim and S.M.L. Agostinho, *J. Electroanal. Chem.*, 535 (2002) 75.
40. Z.V.P. Murthy and K. Visayaragavan, *Green Chem. Lett. Rev.*, 7 (2014) 209.
41. M.E. Mert, G. Kardas and B. Yazıcı, *Corros. Sci.*, 53 (2011) 4265.
42. G. Gece, *Corros. Sci.*, 50 (2008) 2981.
43. M.A. Amin, K.F. Khaled, Q. Mohsen and H.A. Arida, *Corros. Sci.*, 52 (2010) 1684.
44. J. Zhang, J. Liu, W. Yu, Y. Yan, L. You and Linfa Liu, *Corros. Sci.*, 52 (2010) 2059.
45. H.M. Abd El-Lateef, *Corros. Sci.*, 92 (2015) 104.

© 2018 The Authors. Published by ESG ([www.electrochemsci.org](http://www.electrochemsci.org)). This article is an open access article distributed under the terms and conditions of the Creative Commons Attribution license (<http://creativecommons.org/licenses/by/4.0/>).